lutionarily conserved association of Cdc20 and BubR1 with γ-TuRC components. The molecular interaction data, from both *Drosophila* and human cells, suggested a mechanism coupling the spindle assembly checkpoint to γ-TuRC.

Because BubR1 and Cdc20 were in a complex with γ-tubulin, we investigated the functional importance of this interaction for the activation of the spindle checkpoint. A true spindle checkpoint protein is described as a component required for the activation of the checkpoint (*22*). In its absence, cells do not arrest in metaphase but separate sister chromatids and then exit mitosis (*23*, *24*). We used this property of the spindle checkpoint kinases to test whether depletion of γ-tubulin actually triggers a true spindle checkpoint or leads to an increase of the mitotic index through another pathway. The simultaneous knockdown of γ-tubulin and either of the checkpoint kinases described above had (apart from Bub1) a much-reduced mitotic index when compared to the EGFP/γ-tubulin control knockdown (Fig. 2B). This means that these checkpoint proteins were necessary for the γ-tubulin depletion–mediated mitotic arrest, confirming that γ-tubulin triggered a proper spindle assembly checkpoint response. As expected, Bub1 did not show any significant difference in the mitotic rate when compared to the negative control EGFP/γ-tubulin knockdown (Fig. 2B) (*25*). In addition, the simultaneous knockdown between Cdc20 and γ-tubulin increased the percentage of mitotic cells when compared to the Cdc20 single knockdown (Fig. 2B). Thus, the effects of γ-tubulin and Cdc20 depletion are cumulative, and γ-tubulin and Cdc20 interact functionally, which agrees with our biochemical data that γ-tubulin and Cdc20 are in a complex.

The kinetochore is composed of transiently associated proteins such as the checkpoint proteins, as well as more structural proteins [for example, CENP-B, CENP-C, and the histone H3–related protein CENP-A (CID in *Drosophila*)] (*26*). To test the respective contribution of signaling to the checkpoint from γ-TuRC and from the kinetochore, we removed a structural component of the kinetochore in SL2 cells. We achieved this step by using RNAi of the *Drosophila* CENP-A homolog CID (Fig. 3), a protein that is localized in or close to the inner plate of the *Drosophila* kinetochore and is required for kinetochore assembly (*27*). The efficient depletion of CID (Fig. 3, D to F) as compared to control cells (Fig. 3, A and B) caused mitotic arrest (Fig. 3C) and displaced the chromosomes from the metaphase plate (Fig. 3, D to F), suggesting microtubule-kinetochore attachment defects. Knockdown of γ-tubulin together with CID caused a further increase in the mitotic index when compared to single CID knockdown (Fig. 3C). This supports our hypothesis that γ-TuRC depletion is likely to activate an additional spindle checkpoint signal.

It has been suggested that the centrosome serves as a complex platform for multiple cellular signaling pathways (*2*, *3*, *28*). For example, cyclin B degradation, catalyzed through Cdc20, starts on the centrosome, thus functioning as a molecular hub integrating the interaction of proteins that regulate mitotic progression (*28–30*). Here we provide evidence that γ-TuRC proteins, rather than the centrosome per se, play a molecular role in the activation of the spindle checkpoint. We propose that γ-TuRC proteins are integrated in a signaling mechanism at the microtubule minus ends, and they are interacting with spindle checkpoint components independently of centrosome integrity.

References and Notes

1. M. F. Tsou, T. Stearns, *Curr. Opin. Cell Biol.* **18**, 74 (2006).
2. G. Sluder, *Nat. Rev. Mol. Cell Biol.* **6**, 743 (2005).
3. S. Doxsey, W. Zimmerman, K. Mikule, *Trends Cell Biol.* **15**, 303 (2005).
4. D. Job, O. Valiron, B. Oakley, *Curr. Opin. Cell Biol.* **15**, 111 (2003).
5. M. Moritz, D. A. Agard, *Curr. Opin. Struct. Biol.* **11**, 174 (2001).
6. Y. Zheng, M. L. Wong, B. Alberts, T. Mitchison, *Nature* **378**, 578 (1995).
7. K. Oegema *et al.*, *J. Cell Biol.* **144**, 721 (1999).
8. M. Moritz, M. B. Braunfeld, V. Guenebaut, J. Heuser, D. A. Agard, *Nat. Cell Biol.* **2**, 365 (2000).
9. B. R. Oakley, *Curr. Top. Dev. Biol.* **49**, 27 (2000).
10. S. Doxsey, D. McCollum, W. Theurkauf, *Annu. Rev. Cell Dev. Biol.* **21**, 411 (2005).
11. L. Vardy, T. Toda, *EMBO J.* **19**, 6098 (2000).
12. C. Verollet *et al.*, *J. Cell Biol.* **172**, 517 (2006).
13. N. L. Prigozhina *et al.*, *Mol. Biol. Cell* **15**, 1374 (2004).
14. V. Barbosa, M. Gatt, E. Rebollo, C. Gonzalez, D. M. Glover, *J. Cell Sci.* **116**, 929 (2003).
15. N. Colombie *et al.*, *Mol. Biol. Cell* **17**, 272 (2006).
16. K. Li, T. C. Kaufman, *Cell* **85**, 585 (1996).
17. Materials and methods are available as supporting material on *Science* Online.
18. A. Khodjakov, C. L. Rieder, *J. Cell Biol.* **153**, 237 (2001).
19. E. H. Hinchcliffe, F. J. Miller, M. Cham, A. Khodjakov, G. Sluder, *Science* **291**, 1547 (2001).
20. T. L. Megraw, L. R. Kao, T. C. Kaufman, *Curr. Biol.* **11**, 116 (2001).
21. C. L. Rieder, A. Schultz, R. Cole, G. Sluder, *J. Cell Biol.* **127**, 1301 (1994).
22. A. Musacchio, K. G. Hardwick, *Nat. Rev. Mol. Cell Biol.* **3**, 731 (2002).
23. G. J. Kops, D. R. Foltz, D. W. Cleveland, *Proc. Natl. Acad. Sci. U.S.A.* **101**, 8699 (2004).
24. G. K. Chan, S. A. Jablonski, V. Sudakin, J. C. Hittle, T. J. Yen, *J. Cell Biol.* **146**, 941 (1999).
25. M. Bettencourt-Dias *et al.*, *Nature* **432**, 980 (2004).
26. G. K. Chan, S. T. Liu, T. J. Yen, *Trends Cell Biol.* **15**, 589 (2005).
27. M. D. Blower, G. H. Karpen, *Nat. Cell Biol.* **3**, 730 (2001).
28. J. W. Raff, K. Jeffers, J. Y. Huang, *J. Cell Biol.* **157**, 1139 (2002).
29. C. L. Rieder, S. Faruki, A. Khodjakov, *Trends Cell Biol.* **11**, 413 (2001).
30. B. M. H. Lange, *Curr. Opin. Cell Biol.* **14**, 35 (2002).

31. We acknowledge R. Aebersold, I. A. Dawson, G. Goshima, A. C. Gringas, G. Karpen, T. Kaufman, C. Sunkel, R. Vale, W. Whitfield, and Y. Zheng for the gift of antibodies, cells, and DNA constructs; the help of S. Haesler and D. Weichart with parts of the fluorescence-activated cell sorting and IP experiments; and our colleagues and A. Ploubidou for their comments on the manuscript. The work in the laboratory of B.M.H.L. is funded through the Berliner Senat für Kultur, Wissenschaft und Forschung, Project Ultrastructural Network, European Funds for Regional Development; by the Bundesministerium fur Bildung und Forschung, German Network for Genome Research 2, Systematic-Methodological Platform–Protein; by the European Union; and by the Max-Planck Society and the Thyssen Foundation.

Supporting Online Material

www.sciencemag.org/cgi/content/full/314/5799/654/DC1
Materials and Methods
SOM Text
Figs. S1 to S3
References

21 July 2006; accepted 18 September 2006
10.1126/science.1132834

Odorant Receptor–Derived cAMP Signals Direct Axonal Targeting

Takeshi Imai,[1,2] Misao Suzuki,[3] Hitoshi Sakano[1,2]*

In mammals, odorant receptors (ORs) direct the axons of olfactory sensory neurons (OSNs) toward targets in the olfactory bulb. We show that cyclic adenosine monophosphate (cAMP) signals that regulate the expression of axon guidance molecules are essential for the OR-instructed axonal projection. Genetic manipulations of ORs, stimulatory G protein, cAMP-dependent protein kinase, and cAMP response element–binding protein shifted the axonal projection sites along the anterior-posterior axis in the olfactory bulb. Thus, it is the OR-derived cAMP signals, rather than direct action of OR molecules, that determine the target destinations of OSNs.

Each olfactory sensory neuron (OSN) in the mouse expresses only one functional odorant receptor (OR) gene out of ~1000 members (*1–3*). Axons from OSNs expressing a given OR converge onto a specific site, the glomerulus, in the olfactory bulb (*4–6*). It has been proposed that OR molecules at axon termini may directly recognize guidance cues on the olfactory bulb and mediate homophilic interactions of like axons (*6–10*). OR molecules are heterotrimeric guanine nucleotide–binding protein (G protein)–coupled receptors (GPCRs) that transduce the odorant-binding signals by activating the olfactory-specific G protein (G_{olf}) expressed in mature OSNs. The activation of G_{olf} stimulates adenylyl cyclase type III, generating cAMP, which opens cyclic nucleotide–gated (CNG) channels. Mice deficient for G_{olf} and CNGA2 are anosmic but form a normal glomerular map (*11–13*), which suggests that a

G protein other than G_{olf} may aid in targeting OSNs independent of CNG channels.

OR molecules are rhodopsin-like type A GPCRs that contain a conserved tripeptide motif, Asp-Arg-Tyr (DRY), at the cytoplasmic end of transmembrane domain III (fig. S1A), which is required for coupling of GPCRs to the partner G proteins (*14*, *15*). To examine whether the G protein signaling is involved in guidance of OSN axons, we generated a DRY-motif mutant, Arg-Asp-Tyr (RDY), for the rat OR gene *I7* (*16*) and expressed it using a transgenic system (*17*) (fig. S1B). Axons from OSNs expressing the wild-type I7, I7(WT), converged to a specific site in the olfactory bulb (Fig. 1A, left), whereas those expressing the DRY-motif mutant, I7(RDY), remained in the anterior region of the olfactory bulb, failing to converge onto a specific glomerulus (Fig. 1A, right). The I7(RDY)-expressing axons never penetrated the glomerular layer but stayed within the olfactory nerve layer (Fig. 1B). These axon termini were devoid of synaptotagmin (presynaptic marker) and microtubule-associated protein 2 (dendritic marker) immunoreactivities and thus probably did not form synapses (Fig. 2A, middle, and fig. S2). OSNs expressing a nonfunctional OR gene can activate other OR genes and will fail to converge onto a single glomerulus (*8*, *18*, *19*). However, the inability of I7(RDY) axons to converge on a specific glomerulus was not due to the coexpression of other OR genes (fig. S3); OSNs expressing the I7(RDY) transgene expressed no other OR genes. OSNs expressing I7(WT) all showed Ca^{2+} signals in response to octanal (an agonist of the I7 receptor), whereas those expressing I7(RDY) did not (Fig. 1C). Thus, the I7(RDY) mutant is deficient in both axon targeting and G protein coupling.

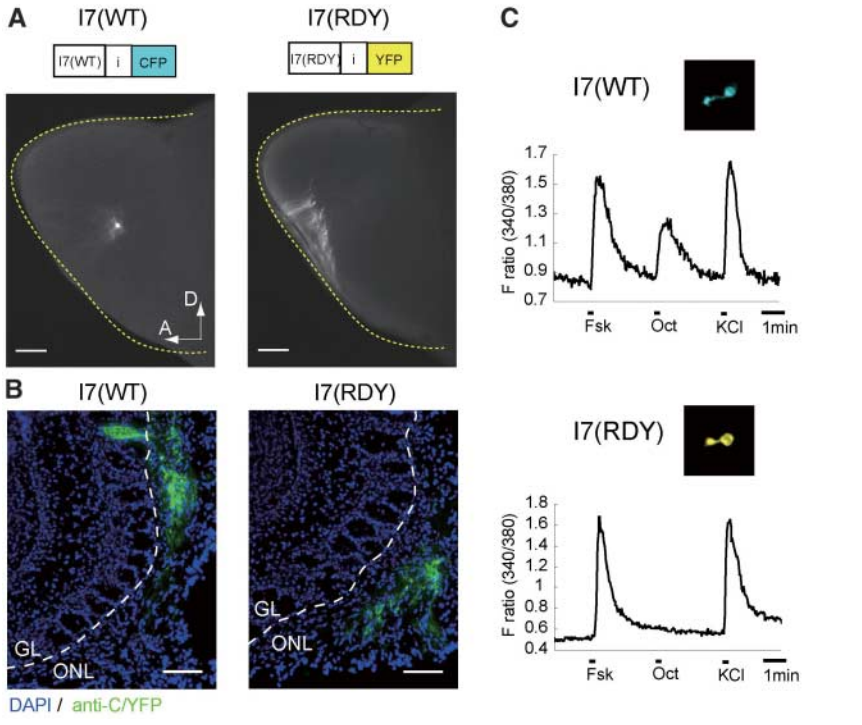

Fig. 1. A DRY-motif mutant of I7 OR. The DRY sequence in the wild-type OR, I7(WT), was changed to RDY in the mutant protein, I7(RDY). (**A**) Whole-mount fluorescent views of olfactory bulbs at postnatal day 14 (P14). Medial aspects are shown. Dotted yellow lines demarcate olfactory bulbs. A, anterior; D, dorsal; i, IRES. Scale bars, 500 μm. (**B**) Coronal sections of olfactory bulbs, stained with antibodies to C/YFP (green) and 4′,6′-diamidino-2-phenylindole (DAPI) (blue). Dashed lines demarcate the olfactory nerve layers (ONL) from the glomerular layers (GL). Scale bars, 100 μm. (**C**) Fura-2 calcium imaging. OSNs responsive to forskolin (an activator of adenylyl cyclase) were analyzed. Cells expressing the I7(WT) all responded to octanal (n = 12 OSNs), whereas those expressing I7(RDY) did not (n = 10). Fsk, 50 μM forskolin; Oct, 500 μM octanal. F ratio (340/380), the ratio of fura-2 fluorescence intensities at 510 nm with excitation at 340/380 nm. Insets show the C/YFP fluorescent images of OSNs analyzed.

[1]Department of Biophysics and Biochemistry, Graduate School of Science, University of Tokyo, Tokyo 113–0032, Japan. [2]Core Research for Evolutional Science and Technology (CREST), Japan Science and Technology Agency, Tokyo 103–0027, Japan. [3]Division of Transgenic Technology, Center for Animal Resources and Development, Kumamoto University, Kumamoto 860–0811, Japan.

*To whom correspondence should be addressed. E-mail: sakano@mail.ecc.u-tokyo.ac.jp

Fig. 2. Rescue of the I7(RDY) phenotype in OSN projection. (**A**) I7(RDY)-caG_s. (**B**) I7(RDY)-caPKA. (**C**) I7(RDY)-caCREB. Whole-mount fluorescent views are shown for the medial surface of the olfactory bulbs (age P14). The source of cAMP signals is schematically shown in (A) for I7(RDY)-caG_s. Coronal sections stained with antibodies to C/YFP (green) and DAPI (blue) are shown below. Synapse formation was examined with antibodies to synaptotagmin (red). Scale bars, 500 μm for the whole-mount bulbs, 100 μm for sections.

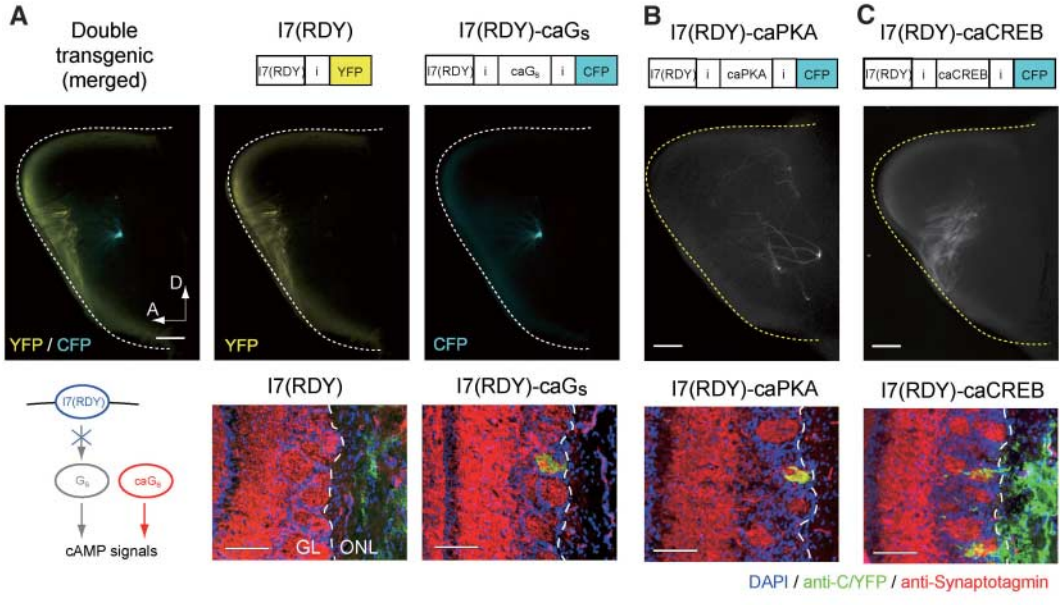

Both G_o and G_s genes are expressed in immature mouse OSNs (*20*). Although the G_s knockout mutation is embryonically lethal (*21*), the G_o-deficient mouse shows no obvious anatomical defect in the olfactory system (*22*). Because the DRY-motif mutant was assumed to be incapable of coupling with G proteins, we examined whether the constitutively active G_s (caG_s) mutant would rescue the defective phenotype of I7(RDY) in axonal projection. We inserted the caG_s gene into the I7(RDY) construct with an internal ribosome entry site (IRES), generating I7(RDY)-caG_s (fig. S1B). In OSNs expressing this construct, cAMP signals should be generated constitutively by caG_s in a receptor-independent manner. Axons expressing I7(RDY)-caG_s (Fig. 2A, cyan) converged to a specific site in the olfactory bulb, whereas axons expressing I7(RDY) (Fig. 2A, yellow) did not. Yellow fluorescent protein (YFP)–positive and cyan fluorescent protein (CFP)–positive axons did not intermingle or co-converge, which suggests that homophilic interaction of OR molecules is unlikely. Axons expressing I7(RDY)-caG_s were found within a glomerular structure and were immunoreactive for synaptotagmin (Fig. 2A, right). G_s stimulates adenylyl cyclase to produce cAMP, which in turn activates cAMP-dependent protein kinase (PKA). A constitutively active PKA rescued the defective phenotype of I7(RDY) in OSN projection and glomerular formation, although a few projection sites were found in the posterior region in the olfactory bulb (Fig. 2B). When the I7(RDY) construct was coexpressed with a constitutively active variant of cAMP response element–binding protein (CREB), a PKA-regulated transcription factor, axon termini were found within glomerular structures, although with incomplete convergence (Fig. 2C). These results confirm the role of G proteins in OSN axon targeting and suggest the involvement of cAMP in transcriptional regulation of axon guidance molecules.

To study cAMP signaling in OSN projection, we examined the effect of caG_s on OSNs expressing the wild-type OR. Two transgenic constructs, I7(WT)-Cre and I7(WT)-caG_s, were analyzed. The *Cre* recombinase gene was assumed not to affect the G_s-mediated signaling. Axons from OSNs expressing I7(WT)-Cre (Fig. 3A, yellow) or I7(WT) (Fig. 3A, cyan) converged in similar regions, whereas those expressing I7(WT)-caG_s (Fig. 3B, left) projected to more posterior regions. Additional cAMP signals are generated by caG_s. In OSNs expressing I7(WT)-caG_s, cAMP signals are generated by both the transgenic caG_s and endogenous G_s, whereas, in OSNs expressing I7(RDY)-caG_s, the generation of cAMP signals by endogenous G_s is blocked. The glomerulus for I7(WT)-caG_s (Fig. 3B, yellow) showed a smaller posterior shift from that for I7(RDY)-caG_s (Fig. 3B, cyan). Thus, the signaling level of the endogenous G_s appears to be relatively low when coupled with the wild-type OR. We also tested whether decreased levels of cAMP signals would affect the OSN projection. Axons expressing a dominant-negative PKA (dnPKA) with the wild-type OR converged to the anterior part of the olfactory bulb (Fig. 3C). Unlike axons carrying I7(RDY), axons expressing the I7(WT)-dnPKA construct generated glomerular structures. These transgenic experiments indicate that increased or decreased levels of cAMP signals shift the glomerular target of OSNs posteriorly or anteriorly, respectively.

To examine the effect of excessive cAMP signals on OSN projection, we generated the transgenic construct, caG_s^{hi}, in which the OR coding sequence has been replaced with the caG_s gene (fig. S1B). More caG_s was translated from the cap-dependent caG_s^{hi} than from the IRES-mediated I7(RDY)-caG_s (*8*). Although we

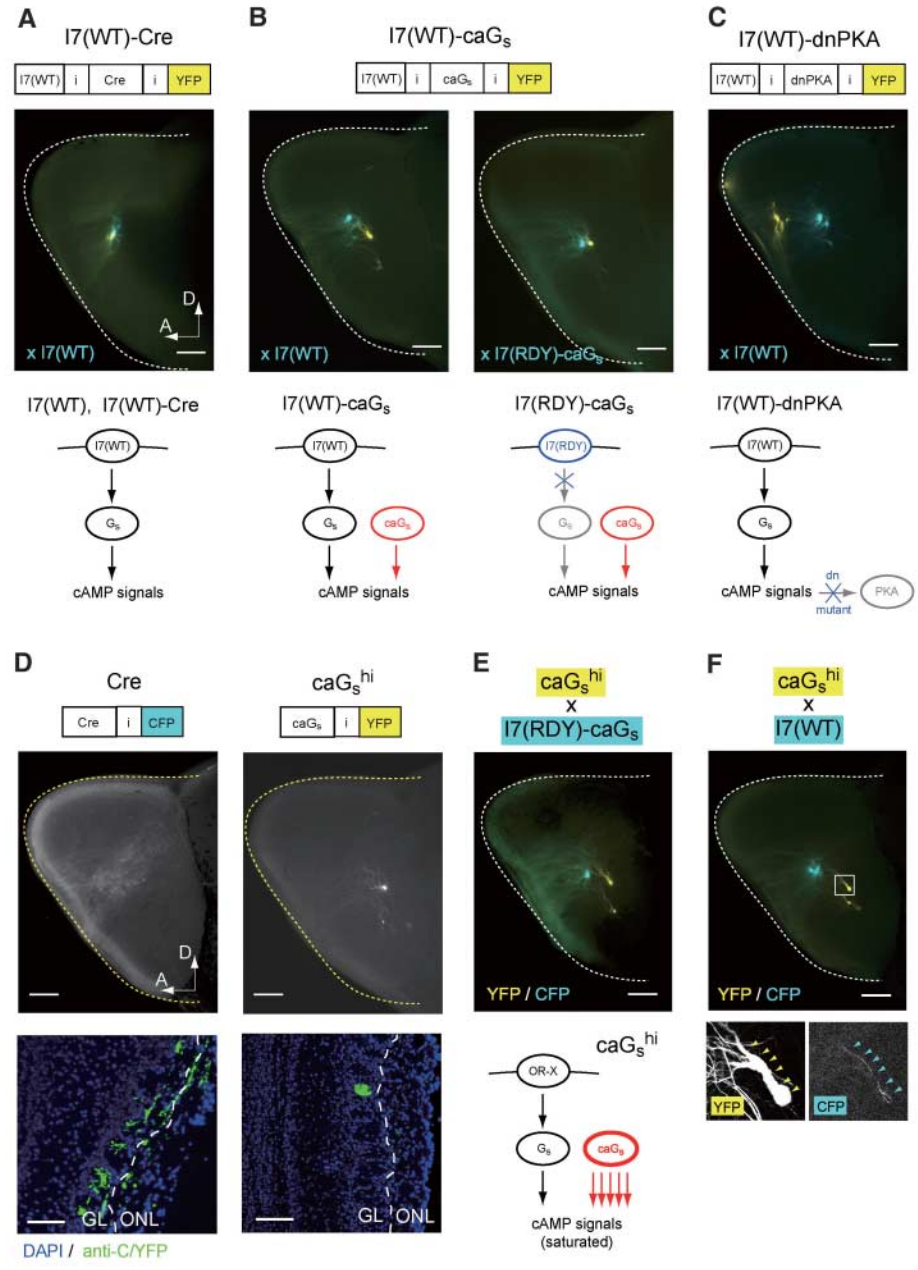

Fig. 3. Genetic manipulations of cAMP signals. Whole-mount fluorescent views of olfactory bulbs (medial surface) were analyzed for various double transgenic mice (age P14). OSN axons expressing the transgenes were visualized with CFP (cyan) or YFP (yellow). (**A**) YFP-tagged I7(WT)-Cre / CFP-tagged I7(WT). (**B**) Left, YFP-tagged I7(WT)-caG_s / CFP-tagged I7(WT); right, YFP-tagged I7(WT)-caG_s / CFP-tagged I7(RDY)-caG_s. (**C**) YFP-tagged I7(WT)-dnPKA / CFP-tagged I7(WT). (**D**) Coding region–replaced transgenic constructs, Cre and caG_s^{hi}. (**E**) CFP-tagged I7(RDY)-caG_s / YFP-tagged caG_s^{hi}. (**F**) YFP-tagged caG_s^{hi} / CFP-tagged I7(WT). Higher power confocal views of the boxed area (insets) are also shown. Arrowheads indicate the trajectories of labeled axons. Sources of cAMP signals are schematically shown for the OSNs expressing the respective transgenic constructs. Scale bars, 500 μm for whole-mount bulbs, 100 μm for sections.

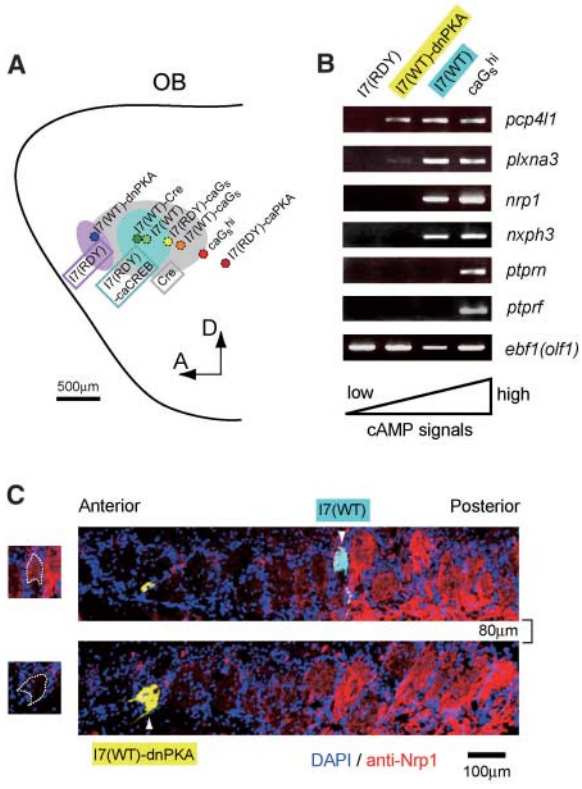

Fig. 4. Glomerular locations and cAMP signal levels. (**A**) Projection sites on the medial surface of the olfactory bulb (OB) are schematically shown for various transgenic constructs (fig. S6B). (**B**) RT-PCR analyses of single OSNs. cDNA libraries were prepared from single OSNs of four different transgenic mice: I7(RDY), I7(WT)-dnPKA, I7(WT), and caG$_s^{hi}$. The genes up-regulated by the cAMP signals were screened with microarray and RT-PCR analyses. Mixtures of 20 single-cell cDNA samples were analyzed by RT-PCR for the expression of isolated genes. Six examples are shown: *pcp4l1*, *plxna3*, *nrp1*, *nxph3*, *ptprn*, and *ptprf*. The gene *ebf1* (*olf-1*) was used as a control. (**C**) Expression profiles of Nrp1 in the olfactory bulb. Two horizontal olfactory bulb sections (80 μm apart) from the I7(WT)/I7(WT)-dnPKA double transgenic mouse (age P14) were immunostained with antibodies to Nrp1 (red). The posteriorly located I7(WT) glomerulus (cyan, arrowhead) was immunoreactive for Nrp1, whereas the anteriorly located I7(WT)-dnPKA glomerulus (yellow, arrowhead) was not. On the left, the I7(WT) and I7(WT)-dnPKA glomeruli (dotted traces) are compared for the Nrp1 expression. Quantitative analyses of glomeruli for Nrp1 expression are shown in fig. S5.

expected a posteriorly shifted but scattered pattern of projection with caG$_s^{hi}$, we detected only one or a few glomeruli (Fig. 3D). Projection sites driven by caG$_s^{hi}$ were located posterior to the I7(RDY)-caG$_s$ glomeruli (Fig. 3E). In situ hybridization and single-cell reverse transcription polymerase chain reaction (RT-PCR) indicate that OSNs expressing caG$_s^{hi}$ express multiple OR species (fig. S3). In the double transgenic mouse carrying CFP-tagged I7(WT) and YFP-tagged caG$_s^{hi}$, a few I7(WT)-expressing axons that probably also expressed caG$_s^{hi}$ projected to the caG$_s^{hi}$ glomerulus (Fig. 3F). Thus, the caG$_s^{hi}$ glomerulus represents a heterogeneous population of axons expressing different ORs. It is possible that caG$_s^{hi}$ produces saturated levels of cAMP signals and generates a distinct glomerular structure regardless of the OR species.

In contrast to G$_{olf}$, G$_s$ is expressed early in OSN differentiation (*11*). Our experiments suggest the involvement of a PKA-regulated transcription factor, CREB, in OSN projection (Fig. 2C). We used microarray and RT-PCR analyses to screen for genes with expression levels correlated with cAMP signals. cDNA libraries were prepared from single OSNs from four different transgenic mice, and gene expression profiles were compared between caG$_s^{hi}$ and I7(RDY) and between I7(WT) and I7(WT)-dnPKA (Fig. 4, A and B). Among the genes differentially expressed were some encoding axon guidance molecules [for example, neuropilin-1 (Nrp1)]. *Nrp1* was expressed in the caG$_s^{hi}$ OSNs (where cAMP signals might be high), but not in the I7(RDY)-expressing OSNs (where cAMP signaling is blocked) (Fig. 4B and fig. S4). Immunostaining demonstrated a gradient of Nrp1 expression, with low expression in the anterior and high expression in the posterior of the olfactory bulb (fig. S5). In the I7(WT) / I7(WT)-dnPKA mouse, the I7(WT) glomerulus (Fig. 4C, cyan, posterior) was Nrp1-positive, and the I7(WT)-dnPKA glomerulus (Fig. 4C, yellow, anterior) was Nrp1-negative. Nrp1 has been implicated in guidance of OSN axons, because the disruption of the *Sema3A* gene, which encodes a repulsive ligand for Nrp1, alters glomerular arrangements along the anterior-posterior axis (*23*, *24*). We suggest that G$_s$-mediated cAMP signals regulate the transcription of genes encoding axon guidance molecules, which in turn guide positioning of glomeruli.

Our results explain some puzzling observations about OSN targeting. The β_2-adrenergic receptor (β_2AR), but not a vomeronasal receptor (V1rb2), can substitute for an OR in OR-instructed axonal outgrowth and glomerular formation (*8*). The explanation for this observation may be that the β_2AR can couple to G$_s$, but the V1rb2 cannot. This explanation is consistent with the idea that the G$_s$-mediated cAMP levels set by the receptors determine the target sites of OSN axons. Another puzzling observation is that alterations in OR expression levels can affect OSN projection (*8*). The level of cAMP signals may be affected by both OR identity and the amount of OR protein, which would be a factor of transcription and translation parameters. OR-instructed G$_s$ signals are not dependent on odorants (*23*), and disruption of G_{olf} or *CNGA2* genes did not affect positioning of glomeruli (*11*–*13*), which suggests that G$_s$-mediated cAMP signaling is distinct from that mediated by odor-evoked neuronal activity. It has been thought that ORs at axon termini may recognize guidance cues on the olfactory bulb and mediate the homophilic interactions of like axons (*6*–*10*). However, our results favor a model in which cAMP signals regulate the targeting of OSN axons along the anterior-posterior axis (fig. S6A). These results complement previous studies indicating that the dorsal-ventral arrangement of glomeruli is determined by the locations of OSNs within the olfactory epithelium (*25*–*27*). We propose that a combination of dorsal-ventral patterning, based on anatomical locations of OSNs, and anterior-posterior patterning, based on OR-derived cAMP signals, establishes olfactory bulb topography. After OSN axons reach their approximate destinations in the olfactory bulb, further refinement of the glomerular map may occur through fasciculation and segregation of axon termini in an activity-dependent manner.

References and Notes

1. L. Buck, R. Axel, *Cell* **65**, 175 (1991).
2. B. Malnic, J. Hirono, T. Sato, L. B. Buck, *Cell* **96**, 713 (1999).
3. S. Serizawa *et al.*, *Nat. Neurosci.* **3**, 687 (2000).
4. K. J. Ressler, S. L. Sullivan, L. B. Buck, *Cell* **79**, 1245 (1994).
5. R. Vassar *et al.*, *Cell* **79**, 981 (1994).
6. P. Mombaerts *et al.*, *Cell* **87**, 675 (1996).
7. F. Wang, A. Nemes, M. Mendelsohn, R. Axel, *Cell* **93**, 47 (1998).
8. P. Feinstein, T. Bozza, I. Rodriguez, A. Vassalli, P. Mombaerts, *Cell* **117**, 833 (2004).
9. G. Barnea *et al.*, *Science* **304**, 1468 (2004).
10. J. Strotmann, O. Levai, J. Fleischer, K. Schwarzenbacher, H. Breer, *J. Neurosci.* **24**, 7754 (2004).
11. L. Belluscio, G. H. Gold, A. Nemes, R. Axel, *Neuron* **20**, 69 (1998).
12. D. M. Lin *et al.*, *Neuron* **26**, 69 (2000).
13. C. Zheng, P. Feinstein, T. Bozza, I. Rodriguez, P. Mombaerts, *Neuron* **26**, 81 (2000).
14. T. P. Sakmar, R. R. Franke, H. G. Khorana, *Proc. Natl. Acad. Sci. U.S.A.* **86**, 8309 (1989).
15. A. Scheer, F. Fanelli, T. Costa, P. G. De Benedetti, S. Cotecchia, *EMBO J.* **15**, 3566 (1996).
16. H. Zhao *et al.*, *Science* **279**, 237 (1998).
17. A. Vassalli, A. Rothman, P. Feinstein, M. Zapotocky, P. Mombaerts, *Neuron* **35**, 681 (2002).
18. S. Serizawa *et al.*, *Science* **302**, 2088 (2003).
19. J. W. Lewcock, R. R. Reed, *Proc. Natl. Acad. Sci. U.S.A.* **101**, 1069 (2004).
20. A. Berghard, L. B. Buck, *J. Neurosci.* **16**, 909 (1996).
21. S. Yu *et al.*, *Proc. Natl. Acad. Sci. U.S.A.* **95**, 8715 (1998).
22. A. H. Luo *et al.*, *Brain Res.* **941**, 62 (2002).
23. G. A. Schwarting *et al.*, *J. Neurosci.* **20**, 7691 (2000).
24. M. Taniguchi *et al.*, *J. Neurosci.* **23**, 1390 (2003).
25. K. J. Ressler, S. L. Sullivan, L. B. Buck, *Cell* **73**, 597 (1993).

26. R. Vassar, J. Ngai, R. Axel, *Cell* **74**, 309 (1993).
27. K. Miyamichi, S. Serizawa, H. M. Kimura, H. Sakano, *J. Neurosci.* **25**, 3586 (2005).
28. This work was supported by the CREST Program of the Japan Science and Technology Agency and by grants from Mitsubishi Foundation, Japan Society for the Promotion of Science (JSPS), and the Ministry of Education, Culture and Science of Japan. T.I. was supported by a predoctoral fellowship of JSPS. We thank A. Miyawaki, R. Sprengel, S. McKnight, and M. Mishina for cDNA clones and T. Yamamori, H. Matsunami, and members of our laboratory for valuable comments.

Supporting Online Material
www.sciencemag.org/cgi/content/full/1131794/DC1
Materials and Methods
Figs. S1 to S6
Table S1
References

27 June 2006; accepted 8 September 2006
Published online 21 September 2006;
10.1126/science.1131794
Include this information when citing this paper.

Molecular Phylogeny and Evolution of Morphology in the Social Amoebas

Pauline Schaap,[1] Thomas Winckler,[2] Michaela Nelson,[3] Elisa Alvarez-Curto,[1] Barrie Elgie,[3] Hiromitsu Hagiwara,[4] James Cavender,[5] Alicia Milano-Curto,[1] Daniel E. Rozen,[1]* Theodor Dingermann,[6,7] Rupert Mutzel,[8] Sandra L. Baldauf[3]†

The social amoebas (Dictyostelia) display conditional multicellularity in a wide variety of forms. Despite widespread interest in *Dictyostelium discoideum* as a model system, almost no molecular data exist from the rest of the group. We constructed the first molecular phylogeny of the Dictyostelia with parallel small subunit ribosomal RNA and α-tubulin data sets, and we found that dictyostelid taxonomy requires complete revision. A mapping of characters onto the phylogeny shows that the dominant trend in dictyostelid evolution is increased size and cell type specialization of fruiting structures, with some complex morphologies evolving several times independently. Thus, the latter may be controlled by only a few genes, making their underlying mechanisms relatively easy to unravel.

Multicellular animals and plants display an enormous variety of forms, but their underlying genetic diversity is small compared with the genetic diversity of microbes. Eukaryotic microbes include a broad range of unicellular life forms, with multiple independent inventions of multicellularity. One of the most intriguing challenges in biology is to understand the reason behind the repeated occurrence of this particular evolutionary stratagem.

The social amoebas, or Dictyostelia, are a group of organisms that hover on the borderline between uni- and multicellularity. Each organism starts its life as a unicellular amoeba, but they aggregate to form a multicellular fruiting body when starved. This process has been best described for the model organism *Dictyostelium discoideum*. The aggregate of up to 100,000 *D. discoideum* cells first transforms into a finger-shaped structure, the "slug." The head region of the slug senses environmental stimuli such as temperature and light and directs the slug toward the soil's outer surface, where spores will be readily dispersed. The slug then stands up to form the fruiting body, or sorocarp. The cells in the head region move into a prefabricated cellulose tube and differentiate into stalk cells that ultimately die. The remaining "body" cells then crawl up the stalk and encapsulate to form spores. Thus, the Dictyostelia display distinct characteristics of true multicellularity, such as cell-cell signaling, cellular specialization, coherent cell movement, programmed cell death, and altruism (*1*, *2*).

Traditionally, social amoebas have been classified according to their most notable trait, fruiting body morphology. Based on this, three genera have been proposed: *Dictyostelium*, with unbranched or laterally branched fruiting bodies; *Polysphondylium,* whose fruiting bodies consist of repetitive whorls of regularly spaced side branches; and *Acytostelium*, which, unlike the other genera, forms acellular fruiting body stalks (*1*).

Despite the widespread use of *D. discoideum* as a model organism (*2*, *3*), the Dictyostelia as a whole are poorly characterized in molecular terms; nearly all currently available data are from a single species. Nonetheless, the social amoebas provide a unique opportunity to understand the evolution of multicellularity (*4*–*6*). A primary and essential prerequisite for this is an understanding of the true phylogeny of the group. Here, we describe the phylogeny of social amoeba species and trace the acquisition of morphological and functional complexity during their evolution.

Nearly complete small subunit rRNA (SSU rDNA) gene sequences were determined from more than 100 isolates of Dictyostelia, including nearly every described species currently in culture worldwide (*7*). Phylogenetic analyses of these data identified four major subdivisions of the group, which we numbered 1 to 4 (Fig. 1 and fig. S1). Group 1 consists of a morphologically diverse set of *Dictyostelium* species. Group 2 is a mixture of species with representatives of all three traditional genera, including all pale-colored species of *Polysphondylium*, at least two species of *Dictyostelium*, and all species of *Acytostelium*. Group 3 is again a diverse set of purely *Dictyostelium* species, also including the single cannibalistic species, *D. caveatum*. The largest group is group 4, which consists almost entirely of *Dictyostelium* species but may also include a clade of two violet-colored species from two separate traditional genera, *P. violaceum* and *D. laterosorum.* With the exception of the violet-colored species, group 4 is a fairly homogeneous set of large robust species, including the model organism *D. discoideum* and the cosmopolitan species, *D. mucoroides*, which appears to be polyphyletic (*8*).

The four SSU rDNA groupings are confirmed by α-tubulin phylogeny (fig. S2) with two exceptions: (i) *A. ellipticum* is only weakly placed with group 2 in the α-tubulin tree (fig. S2), and (ii) the *D. laterosorum* and *P. violaceum* clade is grouped together with *D. polycephalum* as the sister group to a weakly supported group 3 plus group 4 clade (0.64 Bayesian inference posterior probability, 51% maximum likelihood bootstrap, fig. S2). This is in contrast to its position as the exclusive sister lineage to group 4 in the SSU rDNA tree (Fig. 1). The SSU rDNA phylogeny also strongly supports group 1 as the deepest major divergence in Dictyostelia (Fig. 1 and fig. S1), as do analyses of combined SSU rDNA plus α-tubulin nucleotide sequences (fig. S3). However, an alternative root is weakly recovered in the α-tubulin amino acid phylogeny (fig. S2). Thus, the position of the dictyostelid root still requires confirmation, which will probably require multiple additional genes.

A notable feature of both phylogenies is the split of the genus *Polysphondylium*. The violet-colored *P. violaceum* is unequivocally grouped together with *D. laterosorum*, and these two lie together at the base of group 4 (Fig. 1) or in groups 3 and 4 (fig. S2). Meanwhile, the pale-colored polysphondylids are all found nested within group 2 (Fig. 1 and

[1]School of Life Sciences, University of Dundee, DD15EH Dundee, UK. [2]Lehrstuhl für Pharmazeutische Biologie, Universität Jena, Semmelweisstrasse 10, 07743 Jena, Germany. [3]Department of Biology, University of York, Box 373, York YO10 5YW, UK. [4]Department of Botany, Tokyo National Science Museum, Tsukuba Botanical Garden, 4-1-1, Amakubo, Tsukuba-shi, Ibaraki 305-0005, Japan. [5]Department of Environmental and Plant Biology, Ohio University, 307 Porter Hall, Athens, OH 45701, USA. [6]Institut für Pharmazeutische Biologie, Universität Frankfurt, Marie-Curie-Strasse 9, 60439 Frankfurt, Germany. [7]Zentrum für Arzneimittelforschung, Entwicklung und Sicherheit (ZAFES), Frankfurt, Germany. [8]Institut für Biologie, Fachbereich Biologie, Chemie, Pharmazie, Freie Universität Berlin, Königin-Luise Strasse 12-16, 14195 Berlin, Germany.

*Present address: Faculty of Life Sciences, University of Manchester, Oxford Road, Manchester M13 9PT, UK.
†To whom correspondence should be addressed. E-mail: slb14@york.ac.uk